News from the Galactic suburbia: the chemical composition of the remote globular cluster NGC 2419[*]

A. Mucciarelli,[1]† M. Bellazzini,[2] R. Ibata,[3] T. Merle,[4] S. C. Chapman,[5] E. Dalessandro[1] and A. Sollima[6]

[1]*Dipartimento di Astronomia, Università degli Studi di Bologna, Via Ranzani, 1-40127 Bologna, Italy*
[2]*INAF – Osservatorio Astronomico di Bologna, Via Ranzani, 1-40127, Bologna, Italy*
[3]*Observatoire Astronomique, Université de Strasbourg, CNRS, 11, rue de l'Université, F-67000 Strasbourg, France*
[4]*Université de Nice Sophia-antipolis, CNRS (UMR 7293), Observatoire de la Côte d'Azur, Laboratoire Lagrange, BP 4229, 06304 Nice, France*
[5]*Institute of Astronomy, Madingley Road, Cambridge CB3 0HA*
[6]*INAF – Osservatorio Astronomico di Padova, Vicolo dell'Osservatorio 5, I-35122 Padova, Italy*

ABSTRACT

We present the chemical analysis of 49 giant stars of the globular cluster NGC 2419, using medium resolution spectra collected with the multi-object spectrograph DEIMOS@Keck. Previous analysis of this cluster revealed a large dispersion in the line strength of the infrared Ca II triplet, suggesting an intrinsic star-to-star scatter in its Fe or Ca content. From our analysis, we assess that all the investigated stars share the same [Fe/H], [Ca/Fe] and [Ti/Fe] abundance ratios, while a large spread in Mg and K abundances is detected. The distribution of [Mg/Fe] is bimodal, with ∼40 per cent of the observed targets having subsolar [Mg/Fe], down to [Mg/Fe] ∼ −1 dex, a level of Mg deficiency never observed before in globular clusters. It is found that the large dispersion in Mg abundances is likely the main origin of the observed dispersion of the Ca II triplet lines strengths (that can be erroneously interpreted in terms of Fe or Ca abundance scatter) because Mg plays a relevant role in the atmosphere of giant stars as an electron donor. A strong depletion in the Mg abundance leads to an increase of the line strength of the Ca II triplet, due to the variation in the electronic pressure, at a constant Fe and Ca abundance. Finally, we detect an anti-correlation between Mg and K abundances, not easily explainable within the framework of the current nucleosynthesis models.

Key words: stars: abundances – stars: atmospheres – stars: evolution – stars: Population II – globular clusters: individual: NGC 2419.

1 INTRODUCTION

The old and metal-poor cluster NGC 2419 is by far the most luminous globular cluster (GC) residing in the outermost fringes of the Milky Way (MW) halo, ≳10 times brighter than any other cluster having $R_{GC} \geq 40$ kpc, (see Galleti et al. 2007, for discussion and comparison with remote clusters in the halo of M31). This unusual feature, coupled with a half-light radius much larger than that of

ordinary globulars of similar luminosity led several authors to the hypothesis that NGC 2419 can be the remnant of an originally larger system, like a nucleated dwarf galaxy (Mackey & van den Bergh 2005; Brodie et al. 2011).

Since the kinematics and the stellar mass function of NGC 2419 are fully consistent with a typical GC made up of stars and stellar remnants (see Ibata et al. 2011a; Bellazzini et al. 2012, and references therein), the key test to establish the actual nature of the system is to search for inhomogeneities in the abundance of chemical elements heavier than aluminium among member stars. A spread in the heavy elements up to the iron-peak group would indicate that the system was a site of chemical evolution driven by Supernovae (SNe), implying that, at the epoch of SNe explosions, the progenitor of NGC 2419 was sufficiently massive to retain their highly energetic ejecta (>few × 10^6 M$_\odot$; Baumgardt, Kroupa & Parmentier 2008); hence, it was likely a dwarf galaxy. On the other hand, GCs are observed to display virtually no spread in heavy

elements and large (and correlated) spreads in light elements (Na, O, Mg, Al, in particular), likely associated with a spread in He abundance (see Gratton, Carretta & Bragaglia 2012, and references therein). These signatures are generally believed to trace early chemical evolution driven by much less energetic polluters than SNe, like massive asymptotic giant branch stars (AGB; D'Antona et al. 2002; D'Ercole et al. 2008) or fast rotating massive stars (FRMS; see Decressin et al. 2007a; Decressin, Charbonnel & Meynet 2007b, and references therein), whose ejecta can be retained in systems in the plausible range of mass of proto-GCs. The anti-correlation between Na and O abundances is so ubiquitous in GCs (and non-existent in the field) that it has been proposed as a fundamental defining feature for globulars (with respect to open clusters and galaxies; Carretta et al. 2010a).

The large distance of NGC 2419 (87.5 kpc; Di Criscienzo et al. 2011a) has prevented the detailed spectroscopic analysis of a large sample of its stars that is needed to perform this chemical test, until a couple of years ago.[1] Recently Cohen et al. (2010, C10 hereafter) presented the analysis of medium-resolution Keck-DEIMOS spectra around the calcium triplet (near 8600 Å, CaT) for 43 red giant branch (RGB) stars of NGC 2419. Using other GCs of known [Fe/H] as calibrators and adopting a constant [Ca/Fe] value, they translated the measured pseudo-equivalent width of CaT and the magnitude difference between the stars and the cluster horizontal branch (HB, $V–V_{HB}$) into [Ca/H] values, as is usually done for [Fe/H] (see Rutledge, Hesser & Stetson 1997; Battaglia et al. 2008; Starkenburg et al. 2010, and references therein). C10 found a significant spread in the [Ca/H] values derived with this method ([Ca/H]$_{CaT}$ hereafter): the distribution showed a strong peak at [Ca/H]$_{CaT} \simeq -1.95$ and a long tail reaching [Ca/H]$_{CaT} \simeq -1.45$. This relatively large spread in a heavy element (Fe or Ca; see Starkenburg et al. 2010) was interpreted by C10 as providing additional support to the hypothesis that NGC 2419 '. . . is the remnant of a dwarf galaxy accreted long ago by the Milky Way . . .'. As a consistency check C10 obtained Fe and Ca abundances by spectral synthesis of Fe and Ca lines (other than CaT) that are present in their spectra. The puzzling result was that while the Ca abundances are in reasonable agreement with those from CaT, no significant spread in iron abundance was detected.

Available photometry is not of much help in settling this issue, since in this low metallicity regime the sensitivity of optical colours to variations of metallicity is pretty weak. Moreover, even if a tiny colour spread is observed along the RGB, a spread in metallicity is not necessarily the only viable explanation. Di Criscienzo et al. (2011b) used exquisite HST photometry to show that a small but significant colour spread is indeed detected at the base of the RGB; however, this can be fully accounted for by the helium spread that they invoke to reproduce the complex HB morphology of the cluster, within the classical scenario of multiple populations in GCs (Gratton et al. 2012).

Later Cohen, Huang & Kirby (2011, C11 hereafter) used high-resolution Keck-HIRES spectra to derive the detailed abundance of several chemical elements in seven bright RGB members of NGC 2419. Interestingly, (a) the stars studied by C11 do not display any spread in [Fe/H] and [Ca/Fe] in excess to what is expected from the observational uncertainties, and (b) the abundance pattern of these stars is very similar to what is observed in the classical metal-poor GC M30 (NGC 7099), residing in the inner halo of the MW ($D \simeq 8$ kpc, $R_{GC} \simeq 7$ kpc). One of the stars in the C11 sample

(S1131), which is similar to the other six in all other aspects, was found to be extremely Mg deficient ([Mg/Fe] = −0.47) and K rich ([K/Fe] = +1.13), a strong anomaly never reported before, at least in Pop-II stars (see C11 for a detailed discussion). Hence, at present, the results of the chemical test on the nature of NGC 2419 are still not conclusive.

Here we report on the chemical analysis of the medium-resolution Keck-DEIMOS spectra obtained by Ibata et al. (2011a, I11a hereafter) and used, in that paper, for a thorough study of the kinematics of NGC 2419 (see also Ibata et al. 2011b).

2 OBSERVATIONS

In this paper, we analyse spectra collected with the DEIMOS multi-object slit spectrograph mounted on the Keck II telescope. This data set includes spectra of stars located along the RGB and observed with the high-resolution 1200 line mm^{-1} grating coupled with the OG550 filter: the spectra cover the spectral range of 6500–9000 Å with a spectral resolution of ∼1.2 Å. Target selection, observations and the reduction procedure are described and discussed in full detail in I11a.

2.1 Metallicity from CaT

[Fe/H]$_{CaT}$ was derived by I11a for the stars observed with DEIMOS[2] from the pseudo-equivalent width (EW) of the three CaT lines (suitably combined) and $V–V_{HB}$ (see I11a for details). Here we slightly revise these estimates by (a) adopting the most recent and reliable value for V_{HB}, i.e. $V_{HB} = 20.31 \pm 0.01$ from Di Criscienzo et al. (2011a) instead of $V_{HB} = 20.45$ from Harris (1996), as done in I11a, and (b) fully propagating all the observational errors into a final error in [Fe/H]$_{CaT}$ for each individual star. It is worth noting that there is only a tiny difference between the new [Fe/H]$_{CaT}$ and those published in I11a: the new [Fe/H]$_{CaT}$ are larger than the older ones by 0.037 dex on average, with an rms of just 0.0004 dex.

In I11a, [Fe/H]$_{CaT}$ was used as an additional parameter to clean the kinematic sample from interlopers. While it was noted that there was a significant spread in [Fe/H]$_{CaT}$, this result was neither quantitatively assessed nor discussed in detail. In Fig. 1, we present the metallicity distribution from CaT for the 118 stars from the most conservative sample of radial velocity members (their *Sample A*) having valid [Fe/H]$_{CaT}$ in I11a. The distribution is roughly similar to that shown by C10: there is a strong peak at [Fe/H]$_{CaT} \simeq -1.8$ and an extended tail (with a possible shoulder at [Fe/H]$_{CaT} \simeq -1.5$, not seen in the distribution by C10) extending up to [Fe/H]$_{CaT} \simeq -1.4$. Any subtle difference in the metallicity zero-point and in the shape of the distribution between this work and C10 can be ascribed to differences in the adopted calibration and in the sample size (118, or 71 stars, versus 43). Hence, we consider the agreement of our result with that of C10 as satisfying.

In the following, to quantitatively estimate the mean and the intrinsic spread (σ) of a distribution in some elemental ratio [X/Y] (like, e.g. [Fe/H] or [Ca/Fe]) we adopt an algorithm that explores a grid of the ([X/Y],σ) space and searches for the couple of parameters that maximizes the maximum likelihood (ML) function defined as

$$ML([X/Y], \sigma) = \sum_{i=1}^{N} \frac{1}{\sigma_{tot}} \exp\left[-\frac{1}{2}\left(\frac{[X/Y] - [X/Y]_i}{\sigma_{tot}}\right)^2\right] \quad (1)$$

---

[1] Shetrone, Coté & Sargent (2001) provided abundance analysis from high resolution spectroscopy for just *one* star of NGC 2419.

[2] I11a included in their sample also stars from the sample by Baumgardt et al. (2009) for which they took only the radial velocity estimate obtained by the same authors from HIRES spectra.
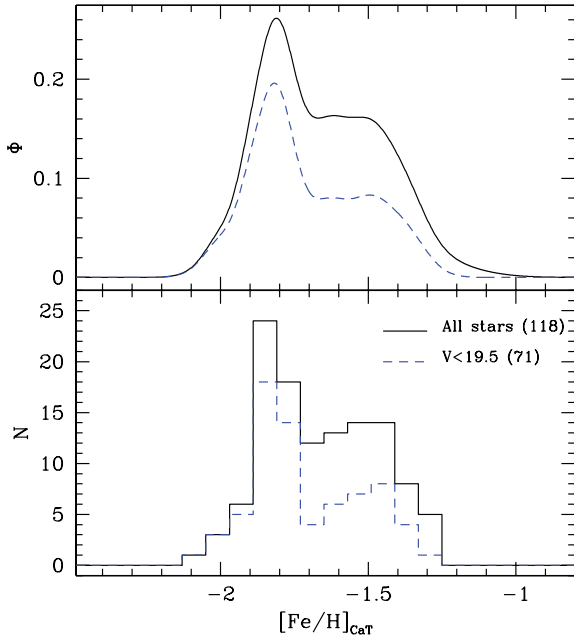
Figure 1. Metallicity distribution derived from CaT, presented as ordinary histograms (lower panel) or as generalized histograms (a representation that removes the effects due to the choice of the starting point and of the bin width; see Laird et al. 1988). Note that the distribution does not change if only the brightest stars are considered (dashed lines).
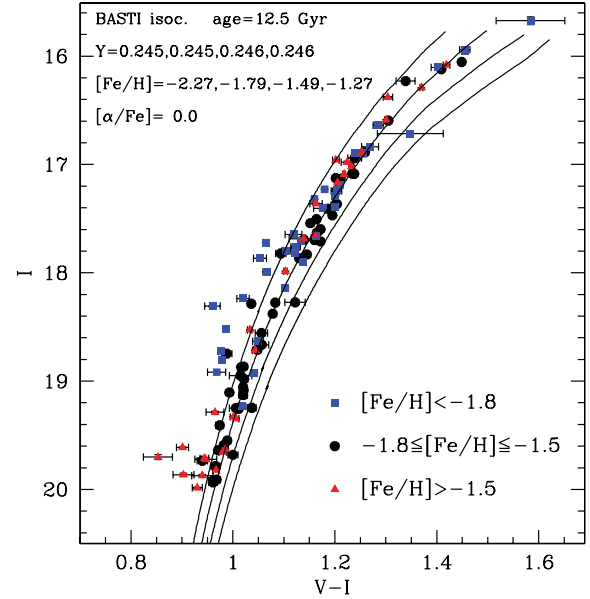

Figure 2. CMD for the 118 stars included in the metallicity distribution from CaT shown in Fig. 1 from the photometric catalogue assembled by Bellazzini (2007) (see Section 2.1). Different symbols are adopted for different metallicity ranges. A grid of isochrones of different metallicity from the BaSTI set is overplotted (Pietrinferni et al. 2004) for reference.

similar to what is currently done to estimate the mean velocity and velocity dispersion in kinematic samples (see, e.g., Walker et al. 2006; Martin et al. 2007). N is the number of stars in the sample and $\sigma_{tot} = \sqrt{\sigma^2 + [X/Y]_{err,i}^2}$, where $[X/Y]_i$ is the abundance of the individual star and $[X/Y]_{err,i}$ is its associated error. The advantage of this approach is that it automatically takes into account the observational errors, thus providing estimates of the *intrinsic spread* with the associated *uncertainty* (derived following Pryor & Meylan 1993), a quantity that is especially valuable in the present contest. Although the adopted ML function is well suited for deriving the parameters of Gaussian distributions, it is clearly not a good approximation for the distribution shown in Fig. 1 (but it turns out to be quite appropriate for the subsequent applications; see Section 3). Nevertheless, it can provide a useful quantitative estimate of the intrinsic spread, that is, $\sigma = 0.17 \pm 0.01$ dex, similar to the massive globular M54 that resides at the centre of the disrupting Sagittarius dwarf galaxy (Bellazzini et al. 2008; Carretta et al. 2010c). A KMM test[3] (Ashman et al. 1994), performed both on the whole sample or on the sub-sample of the brightest stars ($V < 19.5$), finds that a bimodal model is preferred to a unimodal model at the ≥ 99.9 per cent confidence level, and the relative fraction of stars in the two populations is approximately 0.6 and 0.4.

However, the colour–magnitude diagram (CMD) of the target stars shown in Fig. 2 reveals that there are several stars that have *virtually the same magnitude and colour* but that differ by more than 0.3 dex in $[Fe/H]_{CaT}$. The adopted photometry is from the catalogue assembled by Bellazzini (2007) from various sources; however, the B, V, I magnitudes for most of the target stars (and all the stars we analyse with spectral synthesis, below) are taken from the accu-

rate absolute photometry by Stetson (2005). To further investigate this apparent inconsistency between $[Fe/H]_{CaT}$ and photometry, and having in mind the results by C10 and C11, we decided to perform a full spectral synthesis analysis on a subsample of stars of the I11a sample with high signal-to-noise ratio (SNR). This analysis is described and discussed in the following sections.

3 CHEMICAL ANALYSIS

Among the stars recognized as cluster members by I11a in their *Sample A*, we selected stars with sufficient SNR (typically SNR >40 per pixel) to perform a reliable chemical analysis based on spectral synthesis. All the stars have V-band magnitude <18.8 and their position in the CMD is shown in Fig. 3. Even if the sample is clearly dominated by RGB stars, a few AGB stars are likely included. This is not expected to have any effect on the chemical analysis performed below.

3.1 Atmospheric parameters

The atmospheric parameters (T_{eff}, surface gravities and microturbulent velocities) of the target stars cannot be derived directly from the spectra (due to the low spectral resolution and the small number of available lines) and we estimated them from the photometry. Temperatures are computed by employing the empirical $(V - I)_0 - T_{eff}$ transformation by Alonso, Arribas & Martinez-Roger (1999) based on the InfraRed flux method. The dereddened colour $(V - I)_0$ is obtained assuming for all the stars a colour excess of $E(B - V)$= 0.08 ± 0.01 mag (Di Criscienzo et al. 2011a) and the extinction law by McCall (2004). The Alonso et al. (1999) relation for the $(V - I)_0$ colour is computed in the Johnson photometric system; thus, our I Cousin magnitudes have been converted into I Johnson magnitudes by following the prescriptions by Bessell (1979). Internal errors in T_{eff} due to the uncertainties in photometric data and reddening are of the order of about 30–50 K.

[3] The test compares the likelihood of the data for a single Gaussian model and a double Gaussian model and provides the confidence level at which the single Gaussian model can be rejected; see Ashman, Bird & Zepf (1994).
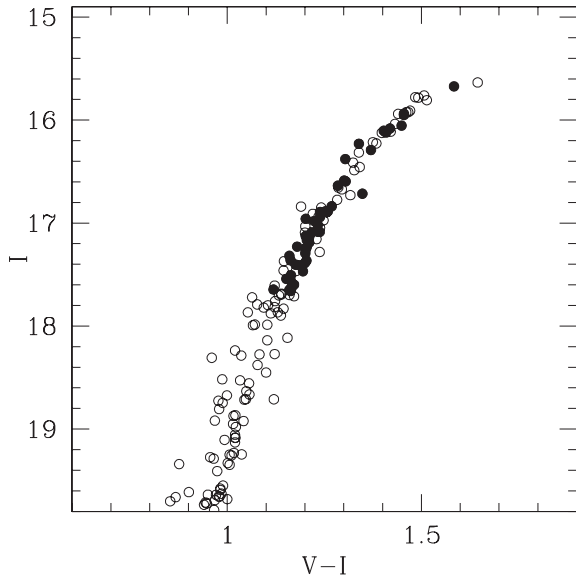
Figure 3. CMD in the $I-(V-I)$ plane of NGC 2419 with the spectroscopic targets analysed here marked as black points. The photometric catalogue is that assembled by Bellazzini (2007); in particular, the source of the photometry for the spectroscopic targets is Stetson (2005).

The surface gravities are computed through the Stefan–Boltzmann relation, assuming the photometric $T_{\rm eff}$, and a typical mass of 0.75 M$_\odot$, according to an isochrone from the BaSTI data set (Pietrinferni et al. 2004) with an age of 13 Gyr, $Z = 0.0003$ and alpha-enhanced ([α/Fe] $= +0.4$ dex) abundance patterns (see C10 and C11). For the luminosities, we used the dereddened V-band magnitudes with the bolometric corrections from Alonso et al. (1999) and the distance modulus of 19.71 ± 0.08 mag (Di Criscienzo et al. 2011a). The gravities can be determined within ± 0.05 dex by propagating the uncertainties in $T_{\rm eff}$, evolutive mass (of the order of 0.05 M$_\odot$), distance modulus and photometry.

Finally, the microturbulent velocities are calculated by adopting the relation between v_t and $\log g$ derived by Kirby et al. (2009): this relation provides values of v_t of $\sim$1.8–2.0 km s^{-1}. Formally, the uncertainties in $\log g$ translate into a typical error in v_t of 0.01 km s^{-1}. Because the majority of the lines analysed here are located in the saturated/damped portion of the curve of growth, these lines are often sensitive to the photospheric velocity fields and we adopted a conservative (and more realistic) error of $\sim$0.2 km s^{-1}. The adopted atmospheric parameters for all the investigated targets are listed in Table 1.

3.2 Model atmospheres and linelist

We began the analysis by employing one-dimensional, local thermodynamic equilibrium (LTE), plane-parallel geometry model atmospheres computed with the code ATLAS9 (originally developed by R L Kurucz) that treats the line opacity through the opacity distribution functions (ODFs) method. The ATLAS9 models are computed by using the ODFs calculated by Castelli & Kurucz (2004) with [M/H] $= -2$ dex, α-enhanced chemical patterns and without the inclusion of the approximate overshooting in the calculation of the convective flux. For some stars with abundance patterns that differ heavily from those adopted in the ODFs computation, specific model atmospheres are computed with the code ATLAS12 that employs the opacity sampling method and allows one to calculate model atmospheres with arbitrary chemical composition (see

Castelli 2005, for a detailed description of the handling of opacity by this code).

Adopting the photometric atmospheric parameters and a guessed metallicity value of [M/H] $= -2$ dex, we calculated synthetic spectra along the entire wavelength range of the observed spectra, including all the atomic and molecular transitions available in the last version of the Kurucz/Castelli linelist.[4] All the synthetic spectra used for the analysis have been generated with the code SYNTHE in its Linux version (Sbordone et al. 2004; Sbordone 2005) and convolved with a Gaussian profile to mimic the spectral resolution of the DEIMOS spectra.

We selected absorption lines that are unblended at the DEIMOS resolution and with the atmospheric parameters and metallicity of our targets. We included in our linelist 19 Fe I lines, 5 Ti I lines, the Mg I line at 8806.7 Å, the CaT line at 8542 and 8662 Å and the resonance K I line at 7699 Å (the other K I transition at 7665 Å being heavily blended with telluric absorption). Reference Solar values are from Grevesse & Sauval (1998).

3.3 Abundance analysis

The traditional derivation of abundances through the measured equivalent widths can be difficult in low resolution spectra, due to the line blanketing conditions that make the continuum location quite complex. Thus, we resort to the comparison with synthetic spectra including all the molecular and atomic transitions. Each selected line has been analysed independently by performing a χ^2 minimization between the normalized spectrum and a grid of synthetic spectra within a spectral window centred around the line (in the case of DEIMOS spectra the typical width of the fitting window is $\sim$4–5 Å). The synthetic spectra were rebinned at the pixel step (0.33 Å pixel^{-1}) of the observations. A preliminary normalization of all the spectra is performed by fitting the entire spectrum with a Chebyshev polynomial. For each line, we adjusted locally the normalization along a region of $\sim$60 Å around the line. When a first abundance is determined from χ^2 minimization, the spectrum is divided by the best-fitting synthetic spectrum and the quotient spectra is fitted with a spline. The resulting spline is used to normalize again the observed spectrum and a new χ^2 minimization is performed [the same approach has been adopted also by Shetrone et al. (2009) and Kirby et al. (2010)].

To derive the Ca abundance we employed a slightly different methodology, by fitting not the entire line profile but only the wings of the two strongest components of the CaT, at 8552 and 8662 Å. The CaT line at 8498 Å has been excluded because its wings are marginally sensitive to the abundance, at variance to the other two lines that are located in the damped part of the curve of growth and they are more sensitive to abundance with respect to saturated lines. We excluded the core region of these features because (i) it is heavily saturated, (ii) it suffers from relevant departures from LTE and (iii) its shape depends on the thermal stratification of the model atmosphere in the outermost atmospheric layers and basically the canonical one-dimensional model atmospheres are not able to describe well the thermal structure of the upper layers where the line core forms.

The K resonance line at 7699 Å suffers from departures from LTE conditions. Unfortunately, large grids of corrections as a function of the atmospheric parameters are not available for this transition.

---

[4] http://www.user.oat.ts.astro.it/castelli/linelists.html

Takeda et al. (2009) and Andrievsky et al. (2010) provided abundances of [K/Fe] computed by including the departures from LTE for GCs and extreme metal-poor halo stars. The magnitude of their corrections agrees very well and, for the resonance line used in our work, the correction is quite small (see fig. 6 in Takeda et al. 2009). Because of the small range of metallicity and T_{eff} of our targets, we decide to apply a unique value (-0.30 dex) of the non-LTE (NLTE) correction for all the targets.

Concerning the CaT lines discussed here, NLTE corrections affect only the core of the lines (as pointed out by Spite et al. 2011; see their fig. 1, but see also Starkenburg et al. 2010 and references therein), while their wings are not affected by the influence of the NLTE and can be used to derive reliable Ca abundances under the LTE assumption. Spite et al. (2011) derived Ca abundances of metal-poor stars by fitting the wings of the CaT lines with both LTE and NLTE profiles, finding that the effect of NLTE on the wings of these lines is negligible (less than 0.1 dex).

Uncertainties in the fitting procedure and in the atmospheric parameters were taken into account and added in quadrature (see Table 1). The uncertainty due to the fitting procedure is computed

Table 1. Identification numbers (from I11a), temperatures, gravities, microturbulent velocities and abundance ratios for the observed stars in NGC 2419.

ID	T_{eff} (K)	log g	v_t (km s^{-1})	[Fe/H]	[Mg/Fe]	[K/Fe]	[Ti/Fe]	[Ca/Fe]
Sun	–	–	–	7.50	7.58	5.12	5.02	6.36
Iba11_54	3989	0.33	2.05	-1.93 ± 0.13	0.24 ± 0.14	0.09 ± 0.21	0.54 ± 0.19	0.24 ± 0.04
Iba11_29	4150	0.52	2.01	-2.09 ± 0.11	0.52 ± 0.12	0.51 ± 0.17	0.27 ± 0.10	0.41 ± 0.05
Iba11_83	4150	0.53	2.01	-2.29 ± 0.12	0.48 ± 0.13	0.63 ± 0.17	0.25 ± 0.13	0.58 ± 0.03
Iba11_57	4159	0.57	2.00	-2.06 ± 0.11	0.49 ± 0.12	0.36 ± 0.17	0.33 ± 0.11	0.44 ± 0.03
Iba11_28	4201	0.60	1.99	-2.09 ± 0.11	-0.74 ± 0.14	1.41 ± 0.17	0.23 ± 0.10	0.50 ± 0.02
Iba11_3	4224	0.62	1.99	-2.16 ± 0.13	0.40 ± 0.13	0.58 ± 0.18	0.25 ± 0.15	0.53 ± 0.02
Iba11_52	4216	0.63	1.99	-2.05 ± 0.11	0.15 ± 0.13	0.67 ± 0.19	0.05 ± 0.11	0.44 ± 0.03
Iba11_21	4323	0.72	1.96	-2.05 ± 0.12	-0.38 ± 0.14	0.67 ± 0.19	0.21 ± 0.14	0.44 ± 0.02
Iba11_44	4274	0.72	1.96	-2.15 ± 0.11	-0.40 ± 0.14	1.26 ± 0.18	0.25 ± 0.13	0.55 ± 0.03
Iba11_159	4381	0.80	1.95	-2.09 ± 0.13	-0.72 ± 0.13	1.88 ± 0.18	0.36 ± 0.12	0.55 ± 0.04
Iba11_36	4387	0.88	1.93	-2.13 ± 0.12	-0.57 ± 0.15	1.64 ± 0.20	0.50 ± 0.13	0.56 ± 0.03
Iba11_112	4380	0.88	1.93	-1.97 ± 0.13	-0.07 ± 0.16	1.46 ± 0.19	0.25 ± 0.10	0.37 ± 0.03
Iba11_164	4414	0.91	1.92	-2.10 ± 0.12	0.50 ± 0.13	0.58 ± 0.20	0.34 ± 0.16	0.43 ± 0.05
Iba11_39	4309	0.90	1.92	-2.17 ± 0.16	0.36 ± 0.18	0.83 ± 0.26	0.22 ± 0.26	0.41 ± 0.05
Iba11_6	4442	1.00	1.90	-2.05 ± 0.13	0.81 ± 0.19	1.01 ± 0.21	0.32 ± 0.21	0.42 ± 0.02
Iba11_82	4471	1.04	1.89	-2.27 ± 0.14	-0.66 ± 0.18	1.30 ± 0.20	0.36 ± 0.25	0.70 ± 0.03
Iba11_35	4460	1.03	1.89	-2.19 ± 0.13	0.49 ± 0.20	0.24 ± 0.21	0.14 ± 0.29	0.53 ± 0.06
Iba11_51	4497	1.05	1.89	-2.15 ± 0.13	0.32 ± 0.18	0.87 ± 0.22	0.25 ± 0.16	0.51 ± 0.05
Iba11_45	4466	1.04	1.89	-2.12 ± 0.14	0.74 ± 0.19	-0.14 ± 0.21	0.17 ± 0.18	0.42 ± 0.08
Iba11_4	4497	1.07	1.88	-1.99 ± 0.13	0.23 ± 0.17	-0.03 ± 0.22	0.03 ± 0.14	0.33 ± 0.03
Iba11_101	4567	1.10	1.88	-1.98 ± 0.14	-1.02 ± 0.19	1.55 ± 0.23	0.12 ± 0.12	0.43 ± 0.05
Iba11_7	4525	1.09	1.88	-1.92 ± 0.13	-0.33 ± 0.21	1.40 ± 0.23	0.41 ± 0.13	0.39 ± 0.04
Iba11_160	4508	1.10	1.88	-2.12 ± 0.13	-0.52 ± 0.24	1.16 ± 0.25	0.34 ± 0.26	0.53 ± 0.02
Iba11_66	4506	1.13	1.87	-2.20 ± 0.13	0.38 ± 0.22	1.25 ± 0.26	0.27 ± 0.18	0.58 ± 0.05
Iba11_119	4499	1.13	1.87	-2.06 ± 0.15	0.14 ± 0.20	0.12 ± 0.23	0.21 ± 0.17	0.42 ± 0.03
Iba11_72	4536	1.14	1.87	-1.95 ± 0.12	-1.33 ± 0.20	1.31 ± 0.23	0.29 ± 0.16	0.43 ± 0.07
Iba11_121	4567	1.17	1.86	-2.17 ± 0.14	0.39 ± 0.23	1.33 ± 0.23	0.29 ± 0.12	0.53 ± 0.06
Iba11_32	4549	1.17	1.86	-1.98 ± 0.13	-0.73 ± 0.22	1.48 ± 0.24	0.37 ± 0.13	0.39 ± 0.03
Iba11_43	4561	1.18	1.86	-2.10 ± 0.12	-0.21 ± 0.19	0.90 ± 0.26	0.41 ± 0.14	0.59 ± 0.02
Iba11_148	4549	1.19	1.86	-2.24 ± 0.14	0.74 ± 0.26	0.29 ± 0.25	0.44 ± 0.17	0.56 ± 0.05
Iba11_89	4610	1.23	1.85	-2.30 ± 0.14	0.82 ± 0.23	0.52 ± 0.26	0.58 ± 0.15	0.53 ± 0.04
Iba11_96	4563	1.21	1.85	-2.18 ± 0.13	–	0.44 ± 0.23	0.38 ± 0.11	0.47 ± 0.05
Iba11_11	4565	1.22	1.85	-2.01 ± 0.14	-0.53 ± 0.22	1.24 ± 0.24	0.29 ± 0.16	0.41 ± 0.03
Iba11_88	4569	1.24	1.84	-2.30 ± 0.12	0.78 ± 0.25	0.20 ± 0.26	0.25 ± 0.23	0.54 ± 0.04
Iba11_69	4651	1.28	1.84	-2.23 ± 0.13	0.61 ± 0.19	1.50 ± 0.24	0.51 ± 0.14	0.44 ± 0.03
Iba11_10	4645	1.29	1.83	-2.00 ± 0.15	-0.73 ± 0.21	1.91 ± 0.24	0.29 ± 0.14	0.53 ± 0.05
Iba11_134	4563	1.26	1.84	-2.02 ± 0.13	0.66 ± 0.22	0.41 ± 0.27	0.22 ± 0.17	0.26 ± 0.09
Iba11_74	4571	1.27	1.84	-2.24 ± 0.13	0.40 ± 0.24	0.80 ± 0.26	0.34 ± 0.21	0.51 ± 0.07
Iba11_1	4618	1.30	1.83	-1.83 ± 0.13	0.51 ± 0.20	0.11 ± 0.26	0.18 ± 0.17	0.14 ± 0.08
Iba11_104	4598	1.29	1.83	-1.98 ± 0.14	0.19 ± 0.22	1.31 ± 0.26	0.22 ± 0.22	0.36 ± 0.03
Iba11_40	4581	1.31	1.83	-2.04 ± 0.13	-1.26 ± 0.24	1.73 ± 0.25	0.28 ± 0.13	0.48 ± 0.05
Iba11_49	4643	1.35	1.82	-2.10 ± 0.15	-0.48 ± 0.27	1.84 ± 0.27	0.27 ± 0.23	0.53 ± 0.03
Iba11_25	4667	1.37	1.81	-2.05 ± 0.13	-0.42 ± 0.26	1.60 ± 0.27	0.05 ± 0.16	0.46 ± 0.07
Iba11_61	4645	1.37	1.81	-2.14 ± 0.15	–	1.08 ± 0.27	0.47 ± 0.18	0.40 ± 0.11
Iba11_158	4626	1.38	1.81	-1.95 ± 0.13	0.77 ± 0.27	0.82 ± 0.26	0.19 ± 0.14	0.33 ± 0.06
Iba11_55	4641	1.40	1.81	-2.12 ± 0.13	0.43 ± 0.24	0.02 ± 0.28	0.09 ± 0.19	0.48 ± 0.05
Iba11_170	4737	1.44	1.80	-1.94 ± 0.13	0.47 ± 0.24	–	0.38 ± 0.14	0.18 ± 0.08
Iba11_90	4651	1.41	1.81	-2.00 ± 0.13	-0.22 ± 0.26	1.34 ± 0.29	0.21 ± 0.19	0.46 ± 0.03
Iba11_46	4645	1.41	1.81	-2.15 ± 0.13	0.81 ± 0.25	0.87 ± 0.29	0.43 ± 0.12	0.39 ± 0.06

by resorting to Monte Carlo simulations: for each spectral line, the Poissonian noise is injected in the best-fitting synthetic spectrum (after the re-mapping at the pixel scale of the observed spectrum) and re-analysed as described above. One hundred Monte Carlo events are computed for each line and the dispersion of the derived abundance distribution is taken to be the 1σ uncertainty. Typically, the uncertainty in the fitting procedure ranges from ± 0.09 dex for SNR = 100 to ± 0.25 dex for SNR = 40. Only for the Ca abundances, the effect of the photon noise is quite small (± 0.02 dex for SNR = 100 and ± 0.05 dex for SNR = 40), because of the large number of pixels used in the χ^2 minimization.

For Fe, Ca and Ti (for which we have measures from different lines), we computed a weighted average abundance for each star by using the error from the Monte Carlo simulations as a weight; for the typical internal uncertainty, we assumed the dispersion of the mean normalized to the root mean square of the number of used lines. For K and Mg (for which one only line is measured), we take the 1σ level of the Monte Carlo distributions as the internal error for each line.

4 CHEMICAL HOMOGENEITY AND INHOMOGENEITY IN NGC 2419

The derived relative abundances of Fe, Mg, Ti, Ca and K for the target stars are reported in Table 1, together with the associated uncertainties. The first issue we want to focus on is the lack of spread in Fe and Ti abundance in our data. Adopting the ML algorithm, we find $\langle$[Fe/H]$\rangle = -2.09 \pm 0.01$ with $\sigma_{\rm [Fe/H]} = 0.00 \pm 0.03$, and $\langle$[Ti/Fe]$\rangle = +0.29 \pm 0.02$ with $\sigma_{\rm [Ti/Fe]} = 0.00 \pm 0.04$. The agreement with the results by C11 is excellent as, with the same algorithm, we obtain $\langle$[Fe/H]$\rangle = -2.08 \pm 0.05$ with $\sigma_{\rm [Fe/H]} = 0.00 \pm 0.08$, and $\langle$[Ti/Fe]$\rangle = +0.28 \pm 0.05$ with $\sigma_{\rm [Ti/Fe]} = 0.00 \pm 0.07$, from their sample of seven stars.[5]

A small intrinsic spread in [Ca/Fe] is detected, $\langle$[Ca/Fe]$\rangle = +0.46 \pm 0.01$ with $\sigma_{\rm [Ca/Fe]} = 0.09 \pm 0.01$, while from C11 we get $\langle$[Ca/Fe]$\rangle = +0.14 \pm 0.06$ with $\sigma_{\rm [Ca/Fe]} = 0.00 \pm 0.07$. The non-null spread in [Ca/Fe] found in our data may be partially due to an underestimate of the errors on the Ca abundance we derive from the wings of the CaT lines, since these lines are in a different part of the curve of growth with respect to all the other lines considered here. Correlation between uncertainties in Fe and Ca abundances may also play a role, as [Ca/Fe] appears to correlate with [Fe/H] even if the spread in [Fe/H] is not statistically significant, while the correlation between [Ca/H] and [Fe/H] is much weaker, if any. This view is supported by the fact that we do not detect an intrinsic spread in [Ca/H]: $\langle$[Ca/H]$\rangle = -1.63 \pm 0.01$ with $\sigma_{\rm [Ca/H]} = 0.00 \pm 0.02$. We conclude that the spread in calcium abundance is absent or very small.

Contrary to Fe, Ca and Ti, large star-to-star spreads in the Mg and K content are detected among the stars of NGC 2419: $\langle$[Mg/Fe]$\rangle = +0.05 \pm 0.08$ with $\sigma_{\rm [Mg/Fe]} = 0.56 \pm 0.06$ and $\langle$[K/Fe]$\rangle = +0.92 \pm 0.08$ with $\sigma_{\rm [K/Fe]} = +0.51 \pm 0.06$. As we shall see in detail below, a single Gaussian model is not appropriate for the observed [Mg/Fe] and [K/Fe] distribution, since these are clearly bimodal. The average and intrinsic spread for [Mg/Fe] are in reasonable agreement with the C11 results ($\langle$[Mg/Fe]$\rangle = +0.29 \pm 0.13$ with $\sigma_{\rm [Mg/Fe]} = 0.30 \pm 0.10$; see Section 5).

---

[5] We have considered here the abundances derived by C11 from TiII lines. From TiI $\langle$[Ti/Fe]$\rangle = +0.12 \pm 0.02$ with $\sigma_{\rm [Ti/Fe]} = 0.00 \pm 0.07$.

C11 provides K abundance only for the anomalous star S1131. The discussion of the K abundances is deferred to Section 6.

The star Iba11_83 was also observed by C11 (star S1209 in their sample): our $T_{\rm eff}$ is lower than that derived by C11 by 200 K and this difference arises mainly from the different colour–$T_{\rm eff}$ transformations and colour excess employed in the two studies. We found that the differences with respect to C11 are basically ascribable to the difference in $T_{\rm eff}$; only for Ca is the discrepancy large. Taking into account the corresponding iron abundances, our Ca abundance is higher than that found by C11 by ~ 0.3 dex, and this difference is only partially explainable with the employed $T_{\rm eff}$ scales. We can suppose that the residual difference is due to the adopted Ca lines.

4.1 Metallicity from CaT in an Mg-deficient atmosphere

The large intrinsic spreads in [Ca/H]$_{\rm CaT}$ and in [Fe/H]$_{\rm CaT}$ reported by C10 and I11a, respectively, and found again in Section 2.1 requires an additional discussion, since our spectral synthesis analysis, in fact, confirmed the results by C11, i.e. there is no intrinsic scatter in iron abundance and just a small (if any) spread in calcium.

The observed large variance of the CaT strength is not due to an Fe or Ca abundance spread but might be explained in light of the large range covered by the Mg abundance. In fact, Mg plays a relevant role in the opacity of cool stars, being one of the most important electron donors, contributing to the formation of the H$^-$ ions, the main source of opacity in these stars together with Fe, Al and the other α elements (the relative contribution of each element depends on the temperature, gravity and optical depth). A depletion of Mg implies a lower number of free electrons available to form H$^-$ ions, leading to a decrease of the H$^-$ opacity. The strength of the CaT lines increases, decreasing the electron pressure (as pointed out by Shetrone et al. 2009). Thus, a large depletion of the Mg abundance produces an increase of the strength of the CaT lines at fixed Ca and Fe abundance.

Fig. 4 shows the comparison of synthetic spectra around the Mg I line (first panel) and the three CaT lines computed by adopting ATLAS12 model atmospheres with $T_{\rm eff} = 4200$ K, $\log g = 0.6$ and [M/H] = -2 dex, and with [Mg/Fe] = $+0.4$ and -1.0 dex (black and red lines, respectively). In the latter case, the strength of the CaT lines significantly increases with respect to the synthetic with [Mg/Fe] = $+0.4$ dex (note that the lines of elements other than Mg and Ca, that are also visible in the spectra, are identical in the two cases). We stress that the two synthetic spectra are identical in terms of overall metallicity, individual abundance patterns (in particular the same Fe and Ca abundances) and atmospheric parameter, and the only difference is in the Mg abundance. Fig. 5 illustrates the behaviour of the electronic pressure and of the temperature as a function of the Rosseland opacity for the two ATLAS12 model atmospheres, where the differences in terms of $T_{\rm eff}$ and P_e are appreciable (in particular in the outermost layers where the core of the CaT lines forms and in the deepest regions where the wings of CaT form).

As a confirmation of this effect, we detect a clear anti-correlation between our [Mg/Fe] abundance ratio and [Fe/H]$_{\rm CaT}$ (Fig. 6). The iron-rich stars (with [Fe/H]$_{\rm CaT} > -1.7$) dex have [Mg/Fe] < 0 dex, and the bimodality in [Fe/H]$_{\rm CaT}$ noted in Section 2.1 reflects the bimodal distribution of Mg abundance (see below).

The link between the Mg abundance and the intensity of the CaT lines is appreciable also in Fig. 7 that compares portions of the spectra for the two target stars Iba11_28 and Iba11_3 (red and black lines, respectively) that have very similar $T_{\rm eff}$ and $\log g$ (see Table 1) and different [Fe/H]$_{\rm CaT}$ (by more than 0.4 dex, but indistinguishable
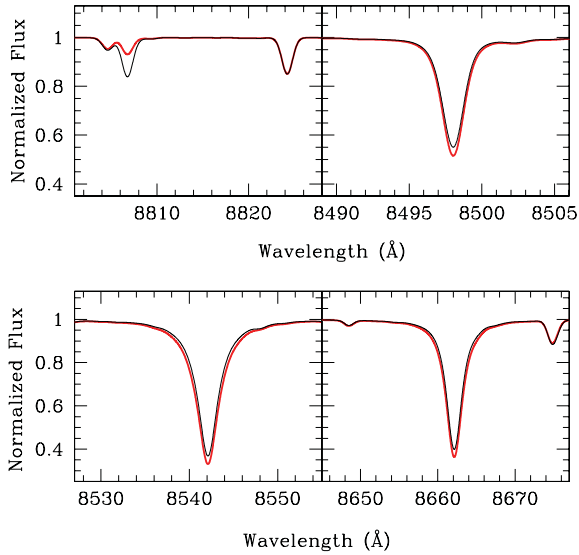
Figure 4. Comparison between the synthetic spectra around the Mg I lines at 8806.7 Å (upper-left panel) and the three CaT lines computed by employing ATLAS12 model atmospheres with T_{eff} = 4200 K, log g = 0.6, [M/H] = −2 dex, α-enhanced patterns, but with [Mg/Fe] = +0.4 dex (black spectrum) and [Mg/Fe] = −1.0 dex (red spectrum). The synthetic spectra are at the same spectral resolution as the DEIMOS spectra.
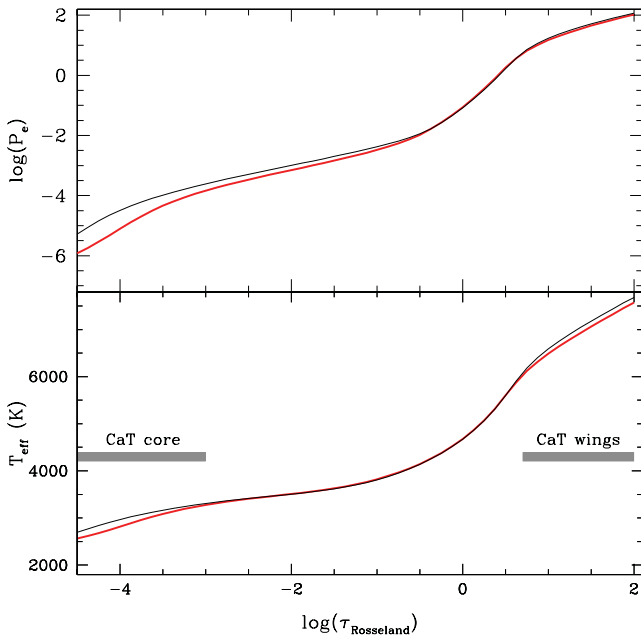

Figure 5. Comparison between the two ATLAS12 models described in the caption of Fig. 4. Upper panel: electronic pressure as a function of the Rosseland optical depth. Lower panel: temperature as a function of the Rosseland optical depth. The grey regions indicate the regions of line formation for the core and the wings of the Ca II triplet.

iron abundance as derived from Fe lines). The difference in the line strength of the CaT line at 8662 Å is evident (upper panel), as well as the difference in the Mg I line in the lower panel. On the other hand, the Fe I lines visible in the spectra are very similar to each other.

Note that the Ca abundances that we derived from spectral synthesis of the wings of the CaT lines take into account the effect of the Mg abundance: the wings were fitted by using synthetic
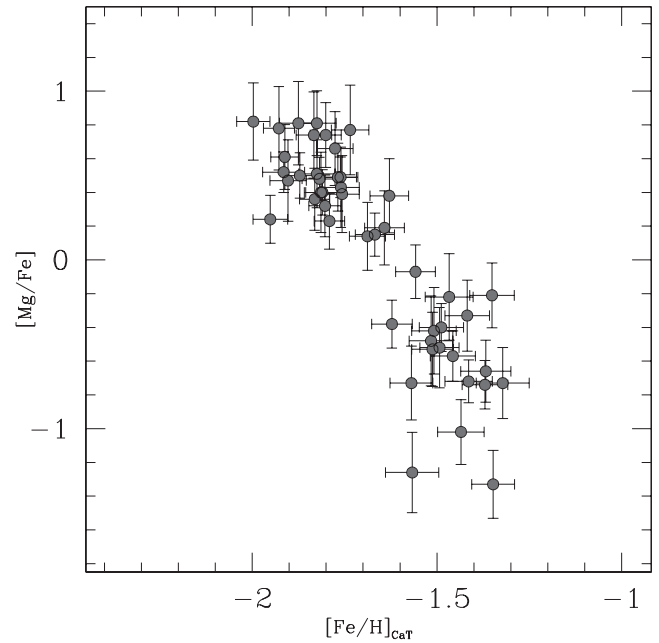
Figure 6. Behaviour of the [Mg/Fe] abundance ratio as a function of the metallicity derived from the CaT lines. The [Mg/Fe] abundances do not include NLTE corrections: as discussed in Section 5, the NLTE corrections are always negative (thus lowering the [Mg/Fe] ratios) and their magnitudes are a function of the Mg abundance: the most Mg-rich stars can be overestimated by 0.2–0.3 dex, while the most Mg-poor stars are basically unaffected by departures from NLTE.
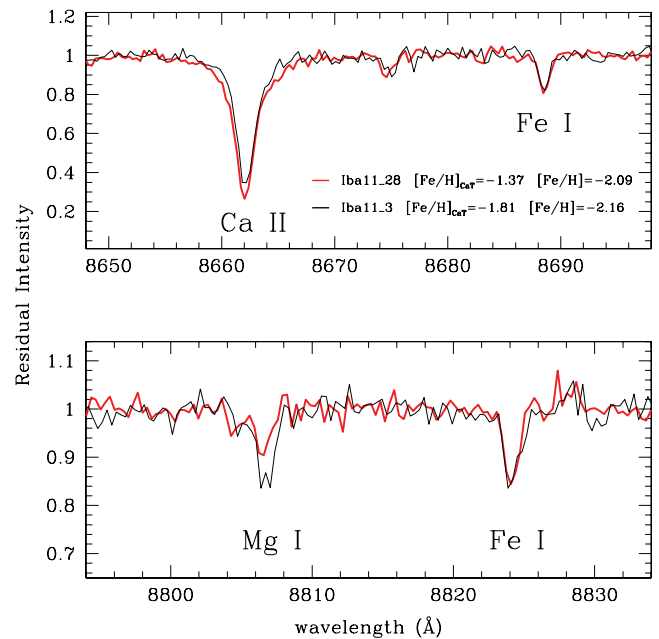

Figure 7. Comparison between the spectra of the stars Iba11_28 (red line) and Iba11_3 (black line) around the CaT line at 8662 Å (upper panel) and around the Mg I line at 8806.7 Å. Note that the two spectra have very similar atmospheric parameters but different [Fe/H] based on the CaT lines. In particular, they have T_{eff} = 4201K and T_{eff} = 4224K, log g = 0.60 and log g = 0.62, respectively, and the same value of microturbulent velocity, v_t = 1.99 km s^{-1}.

spectra computed with the corresponding Mg abundance derived from our analysis[6]. When we repeated the fitting procedure by using only synthetic spectra with [Mg/Fe] = +0.4 dex (the value of the employed ODFs), the Ca abundance of the Mg deficient stars are over-estimated by about 0.2–0.3 dex. This difference is smaller than the Ca abundance range found by C10 (spanning about 0.6–0.7 dex) because the measurement of the equivalent widths of these lines also includes the contribution of the line core that is highly affected by the variation of the electronic density (see Fig. 4) but less sensitive to the Ca abundance.

The Mg depletion observed among the stars of the cluster might explain both the large distributions of [Ca/H]$_{CaT}$ by C10 and of [Fe/H]$_{CaT}$ by Ibata et al. (2011a). As additional confirmation of this interpretation, the Mg-poor star S1131 discussed by C11 has also one of the highest [Ca/H]$_{CaT}$ values in the whole C10 sample.

Finally, we stress that the strength of CaT lines depends on the *global* budget of the free electrons; thus, in addition to Mg, other elements that are electron donors in the atmospheres of cool stars can contribute to shape the CaT lines. In particular, the Al abundance deserves a note of caution, since in ordinary GCs [Al/Fe] anti-correlates with [Mg/Fe] (Gratton et al. 2012). In principle, an enhancement of Al abundance leads to an increase of the free electrons, that could counterbalance those lacking because of Mg depletion. This may be a source of concern for the interpretation of the abundance spreads derived from CaT presented above, since, unfortunately, we lack Al abundance for our target stars. We investigated the effect of different Al abundances (in the range $0.0 \leq$ [Al/Fe] $\leq$ +1.5) coupled with an Mg depletion ([Mg/Fe] = −1) on the strength of CaT lines, using suitable ATLAS12 model atmospheres. We found that the strength of CaT decreases appreciably only for [Al/Fe] $\geq$ 1 dex, thus mitigating the effect of the Mg depletion only in this extreme regime. It is interesting to note that C11 finds an Al abundance much lower than this for the only Mg-deficient star in their sample, S1131 ([Al/Fe] = +0.45). Assuming that this value is representative for the Al abundance in Mg-deficient stars of NGC 2419, the effect on the CaT lines should be negligible.

5 MAGNESIUM DEPLETION

The stars in our sample appear to belong to two groups, according to their Mg abundance (see Figs 6 and 9). A first group is more or less in the range covered by stars in other GCs, $0.0 \lesssim$ [Mg/Fe] $\lesssim$ +0.8 dex (Carretta et al. 2009). Consequently we will dub these stars *Mg normal*. The second group is made of *Mg-deficient* stars having $-1.4 \lesssim$ [Mg/Fe] $\lesssim$ 0.0 dex, a range usually not reached by stars in Galactic globulars (see below). The KMM test confirms that the [Mg/Fe] distribution is bimodal with a confidence level >99.9 per cent. A fraction of 62 per cent of the stars are attributed to the Mg-normal population, having ⟨[Mg/Fe]⟩ = +0.47 dex, and the remaining 38 per cent to the Mg-deficient population, having ⟨[Mg/Fe]⟩ = −0.62 dex.

Intrinsic dispersions in the Mg abundance are usually observed in GCs and explained in the framework of self-enrichment processes, occurring in the early stages of GC evolution. The majority of the MW GC stars for which Mg abundances are available covers a range from +0.2 to +0.5 dex, the only known clusters having Mg-deficient

stars are NGC 2808, where *three* RGB stars with [Mg/Fe] between −0.3 and −0.1 dex have been detected (Carretta et al. 2009), and M54 that harbors two Mg-poor stars (Carretta et al. 2010c). Note that NGC 2808 is characterized by a huge Na-O anti-correlation, with the presence of super O-poor stars, and (likely) a wide and multi-modal distribution in He abundances (D'Antona et al. 2005; Piotto et al. 2007; Bragaglia et al. 2010). Also two RGB stars with [Mg/Fe] = −0.21 and −0.31 dex have been measured in the Large Magellanic Cloud old GC NGC 1786 (Mucciarelli et al. 2009) and both the stars share a very large (<−0.4 dex) depletion of [O/Fe]. Hence, Mg-deficient stars are rare in GCs and seem to be linked to the hypothesized second generation of stars formed from the ejecta of massive AGB stars (D'Ercole et al. 2008) or FRMS (Decressin et al. 2007b) of the first generation, and characterized by high helium and sodium content and strong depletion of O and Mg (see Gratton et al. 2012, and references therein).

Recent analyses of the bimodal HB morphology of NGC 2419 (Dalessandro et al. 2008; Sandquist & Hess 2008) show that a relevant fraction (∼30 per cent) of the HB population is composed of extremely hot stars which have been tentatively interpreted as second-generation stars with high helium content ($Y = 0.42$) by Di Criscienzo et al. (2011b). The fraction of these extreme HB/Blue Hook stars is fairly similar to the fraction of Mg-deficient stars observed in our sample, and the postulated bimodality in the He content is intriguingly reminiscent of the bimodal distribution of [Mg/Fe] detected here.

However, the range of [Mg/Fe] covered by our stars is much larger than anything ever seen before in any stellar system. Hence, while we will come back to discuss the possible physical origin of this feature in Section 8, it is worth discussing briefly some details of the analysis that may lead to erroneous estimates of [Mg/Fe].

In Fig. 7, it is clearly shown that large differences in the strength of Mg lines are observed in the spectra of stars with the *same* atmospheric parameters[7]; hence, some factors other than a variation in these parameters should be responsible of the large star-to-star differences in Mg lines. This is also confirmed by the upper panels of Fig. 8, showing that there is no discernible trend between Mg abundance and T_{eff} and log g. Systematics in the estimates of the micro-turbulent velocity (the only atmospheric parameter that we cannot derive directly from photometry) does not seem able to produce spurious underestimates of the Mg abundance. In fact, the Mg lines for stars of similar T_{eff} and log g are distributed in both the linear and saturated portion of the curve of growth: the weakest lines (those with anomalous low Mg abundances) are those basically unaffected by the velocity fields. Changes in microturbulent velocities will change the Mg abundance for the Mg-rich stars but will have a small or negligible impact on the Mg-poor stars.

Furthermore, the lack of trend of the [Mg/Fe] ratio as a function of T_{eff} and log g suggests that NLTE effects play a negligible role and they are not responsible for the observed Mg range. As pointed out by Merle et al. (2011), the NLTE corrections (in the sense $A_{NLTE} - A_{LTE}$) of the Mg line for a giant star with [M/H] = −2 dex and α-enhanced chemical mixture are negative; hence, the application of the correction would lead to even lower Mg abundance for Mg-deficient stars.

In order to check the magnitude of the NLTE corrections for this Mg line, we calculated the departures from LTE by using a modified

---

[6] For the sake of completeness we repeated the analysis of all the stars with [Mg/Fe] < −0.2 dex by using ATLAS12 model atmospheres computed with the corresponding abundances. Basically, the difference with respect to the analysis performed with the ATLAS9 models is of a few hundredths of dex.

[7] The considered stars differ by just 23 K in the adopted T_{eff}, by 0.02 dex in log g and by 0.0 km s^{-1} in v_t, that is significantly less than the uncertainties in each parameter.
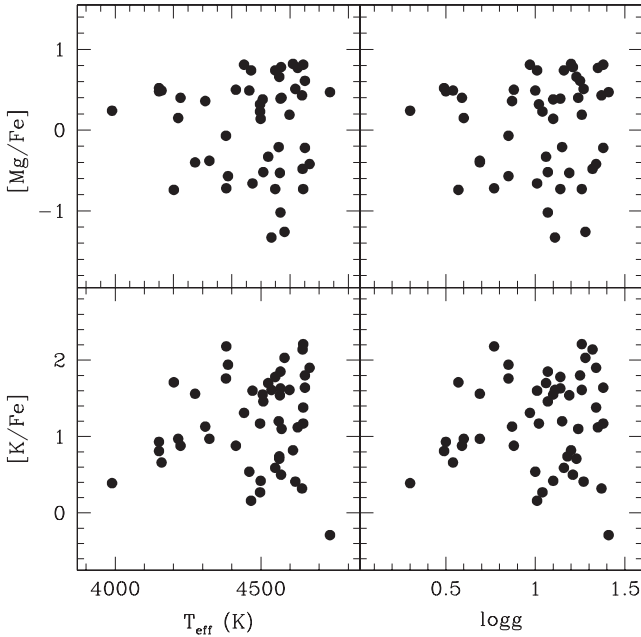
Figure 8. Behaviour of [Mg/Fe] (upper panels) and [K/Fe] (lower panels) abundance ratios as a function of T_{eff} (left-hand panels) and $\log g$ (right-hand panels).

version of the NLTE radiative transfer code MULTI (Carlsson 1986) and α-poor MARCS model atmospheres (Gustafsson et al. 2008) with the typical parameters of our targets: $T_{eff} = 4250$ K, $\log g = 1.5$ and [Fe/H] = −2. We used a simplified model atom of Mg I with 15 energy levels, 26 radiative bound–bound transitions and 91 electron collisional bound–bound transitions (the atomic data are the ones used in Merle et al. 2011). We assumed no contribution from inelastic collision with hydrogen: this will produce upper limits in NLTE abundance corrections. The magnitude of the corrections decreases for lower Mg abundances, because the line is formed progressively deeper in the photosphere, reducing the contribution of the core (where the deviations from LTE are more relevant): for [Mg/Fe] = −1 dex, the NLTE correction is <0.1 dex and the line profile is basically the same under both LTE and NLTE assumptions, while the maximum correction (−0.35 dex) is for high Mg abundances. Thus, we can exclude that the very low [Mg/Fe] values are due to NLTE effects. On the other hand, proper NLTE corrections may lower the Mg abundance of the most Mg-rich stars in our sample, thus leading to an upper limit in the [Mg/Fe] distribution of NGC 2419 more similar to that observed in other Galactic GCs of comparable metallicity (see Fig. 10). Lacking a sufficiently fine grid of NLTE corrections, we are forced to neglect this factor: the reader must be aware that the Mg abundance of stars having [Mg/Fe] $\gtrsim$ +0.5 can be overestimated by 0.2–0.3 dex.

As a sanity check of the Mg indicator used here, we analysed the DEIMOS spectrum of the star S1131 (kindly provided by Kirby and Cohen) that C11 identify as Mg-poor through the measurements of other Mg lines. When the atmospheric parameters by C11 are adopted, we derive [Mg/Fe] = −0.35±0.13 in perfect agreement with the HIRES results. We note that our T_{eff} scale is slightly hotter than that used by C11 (due to the adopted reddening value and T_{eff}–colour transformations). Still, if we derive the atmospheric parameters for S1131 following the same procedure adopted for the stars in our sample, as described in Section 3.1, we obtain [Mg/Fe] = −0.27 ± 0.13, again in good agreement with C11. We stress that

the [Mg/Fe] estimates by C11 and by us for S1131 are based on different Mg lines and the slightly higher abundance derived from the Mg line at 8806.7 Å can be easily explained by taking into account the NLTE effects (note however that the two values are fully consistent within the errors, the actual difference being 0.08 dex).

Finally, we checked the impact of a strong helium enhancement and compare synthetic spectra computed by using ATLAS 12 model atmospheres with normal Y abundance ($Y = 0.24$) and with $Y = +0.4$. The net effect of a high Y value is to make the lines deeper (especially for the strong features) but this effect is very small (typically less than 0.5 per cent of the line depth computed with normal Y) and totally negligible in the analysis of real spectra. Note that the assumption of $Y = +0.4$ does not modify the line profile of the Mg I line at 8806.7 Å; thus, we rule out that the strong depletion of Mg abundance is due to the effect of a very strong He enhancement.

Unfortunately, we cannot measure other elements involved in the chemical anti-correlations typical of GCs (Carretta et al. 2010a). O and Al cannot be detected at this spectral resolution, and the only Na transitions available in our spectral range are the doublet at 8183−94 Å, that is, heavily contaminated by telluric lines (we highlight that the cleaning of telluric lines at this resolution can be quite imprecise). We cannot assess if the Mg depletion is linked to variations of the other light elements. However, the very large Mg distribution of NGC 2419 could be the clue of a peculiar star formation history of the cluster and indicate extremely extended anti-correlation patterns.

6 AN Mg–K ANTICORRELATION?

Fig. 9 displays the clear and significant anti-correlation between [Mg/Fe] and [K/Fe] that occurs in our sample. C11 dedicated a detailed description to their star S1131, labelled as 'a star with a peculiar abundance pattern, characterized by Mg depletion ([Mg/Fe] = −0.47 dex) and K enhancement ([K/Fe] = +1.13 dex). These
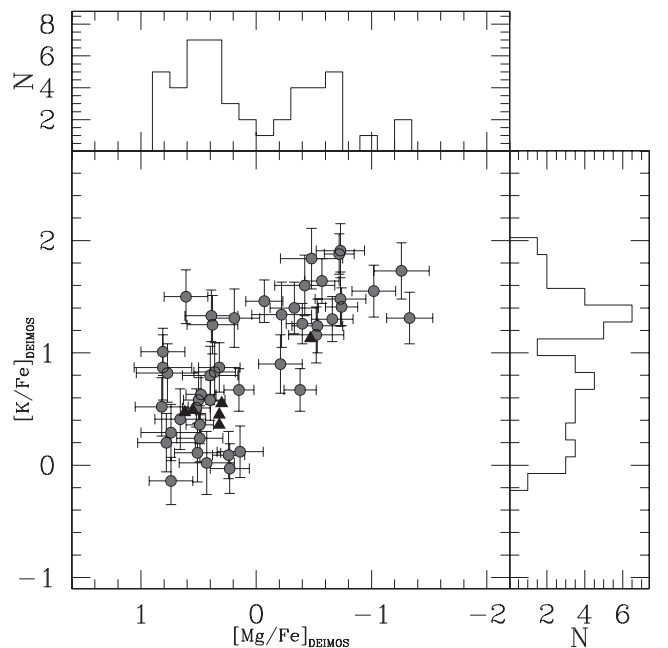

Figure 9. Behaviour of [K/Fe] abundance ratios as a function of [Mg/Fe] ratios. The black triangles are the stars analysed by C11. The histograms of the [Mg/Fe] and [K/Fe] distributions are also plotted.

abundances nicely match those obtained in our analysis (the stars analysed by C11 are plotted for reference in Fig. 9 as black triangles). Taking advantage of our sample of 49 stars, we can assess that this star is not an isolated case, but it belongs to a sub-population of stars in NGC 2419 characterized by sub-solar [Mg/Fe] ratios and high (>1 dex) [K/Fe] ratios.

We investigated some technical reasons that may be able to mimic the observed anti-correlation.

(i) *Contamination by telluric lines.* The used K line is located near the red side of the telluric absorption A band; hence, it may be prone to some contamination. We checked accurately for possible blending with telluric lines, by using as template the DEIMOS spectrum of a rapidly rotating white dwarf. In all the spectra, the K line is free from telluric lines. The Mg line is far from any telluric feature.

(ii) *Errors in the atmospheric parameters.* Both the K and Mg abundance are virtually insensitive to the adopted gravity (at a level of ±0.01 dex for a variation of $\delta \log g = \pm0.1$). The abundances are more sensitive to the $T_{\rm eff}$: a variation of ±50 K translates into a variation of the Mg number density of ±0.06 dex and of the K number density of ±0.1 dex. The errors in $T_{\rm eff}$ can lead a correlation between the Mg and K abundances but are not able to mimic a spurious anti-correlation. In our analysis, v_t is not constrained spectroscopically (as is usually done) but we adopted an empirical relation between v_t and $\log g$. A variation of ±0.2 km s^{-1} leads to a variation of ∓0.08 and ∓0.14 dex in Mg and K abundance, respectively. Also in this case, the errors run in the same direction and are not able to introduce an anti-correlation.

(iii) *Temperature scale.* We checked the impact of a different $T_{\rm eff}$ scale, assuming the temperatures inferred by projecting the position of each target in the CMD on the best-fitting isochrone (see Section 3.1). The average difference between the two scales is $T_{\rm eff}^{\rm isochrone} - T_{\rm eff}^{\rm Alonso99} = -97$ K ($\sigma = 52$ K). The chemical analysis with this $T_{\rm eff}$ scale does not significantly change the observed dispersions both in Mg and K abundances, and does not erase the Mg–K anti-correlation.

(iv) *Departures from LTE.* We applied a unique NLTE correction to all the targets, following the work by Takeda et al. (2009). The NLTE corrections are usually a function of the metallicity and the atmospheric parameters: we note that stars in our sample with the same parameters exhibit different K abundances, suggesting that our NLTE correction is not the cause of the large dispersion in the abundance of potassium.

The two elements are mainly produced by massive stars: K comes from hydrostatic oxygen shell burning and explosive oxygen burning, while Mg is produced by hydrostatic carbon burning and explosive neon burning. However, it is noteworthy that the current yields for K are inadequate to reproduce the observed chemical patterns in the MW (see Romano et al. 2010). Also Mg is destroyed through the Mg–Al cycle of the hot CNO chain in AGB stars. However, the production of K through the proton capture on Argon nuclei could occur in the nucleosynthesis chains of massive AGB stars. Unfortunately the uncertainties related to the cross-sections of these reactions prevent any reliable predictions; preliminary computations indicate that a simultaneous variation of the initial argon abundance and of the cross-section of the proton–argon capture can produce ejecta as enriched in K as we observe in the atmosphere of the Mg-deficient stars (Ventura and D'Antona, private communication).

Takeda et al. (2009) identify two K-rich stars in GCs M4 and M13, coupled with emission components along the Hα line profile. These findings suggest an increase of the velocity fields in the upper

photospheric layers where the core of the K I line at 7699 Å forms. On the other hand, C11 ruled out this hypothesis, because some stars with normal K abundances exhibit Hα emissions larger than those observed in the K-rich star S1131. Unfortunately, the setup of our spectra does not include the Hα line and we cannot check this possibility. In any case, a rise of the turbulent velocity field in the outermost layers of the photosphere should also affect the core of Mg I at 8806.7 Å in a similar fashion.

Finally, we note that the two employed transitions have very different excitational potentials (0 and 4.34 eV for the K and Mg lines, respectively); thus, they formed in different photospheric layers. In fact, the formation of low-χ lines is favoured in external layers, due to the decrease of the temperature with depth, while high-χ transitions occur preferentially in the deepest photospheric regions. In particular, the wings of the two lines form at similar depths, while the formation depth of the core is shifted towards low τ, thus decreasing χ (for comparison, see fig. 13.4 in Gray 1992). The K line forms in the outermost photospheric region where the thermal fluctuations can be relevant (in contrast to the Mg line that forms deeply). Also, temporal variations of the thermal structure of the photosphere cannot be excluded and they could introduce an additional scatter in K abundances but they do not totally explain the anti-correlation with Mg. In any case, the observed spread in potassium requires an independent confirmation using other lines, as well as a search for the Mg–K anti-correlation in other clusters.

7 A COMMENT ABOUT CAT

The CaT represents a widely used indicator of metallicity, especially for distant stellar populations, for which high SNR, high resolution spectra are not easy to achieve. Basically, the combined EW of the CaT lines is a function of the metallicity and it is interpreted in terms of [Ca/H] or [Fe/H] (see Starkenburg et al. 2010, and references therein).

From a theoretical point of view, the strength of the CaT lines is sensitive not only to the abundance of Ca (of course) and Fe, but also to the abundance of those elements that affect the H$^-$ continuum opacity, through their contribution to the electronic density. Basically, the calibrations of the CaT EWs are referred only to cases where all α-element abundance patterns are described by a unique value: for instance, stars with the same level of enhancement of each α element. The [α/Fe] value sets not only the abundance of each α element but also the free electron density, which has a relevant impact in the continuum opacity of cool stars (as discussed above). Spurious cases, where the α elements have largely different patterns to each other, are not taken into account in the usual CaT calibration, but, as demonstrated by the case of NGC 2419, they may lead to a wrong interpretation of the CaT strengths. In fact, CaT can be used as a diagnostic of the metallicity only for stars with *canonical* chemical composition, while the method fails with stars with a peculiar or exotic chemical mixture, because the effective global budget of the free electrons is not taken into account.

Mg deficiencies as extreme as those observed here seem to be very rare in nearby stellar systems (see Fig. 10, and a discussion in C11, Sections 5 and 8). Therefore, it is unlikely that their metallicity distributions derived from CaT are seriously biased by this effect. However, in principle, observed dispersions of CaT in GCs (or dwarf galaxies) can be due not only to (i) an intrinsic variation of Fe (under the assumption that all the stars share the same α content), (ii) an intrinsic variation of Ca (under the assumption that the abundances of the electron donors do not vary from star to star), but also to
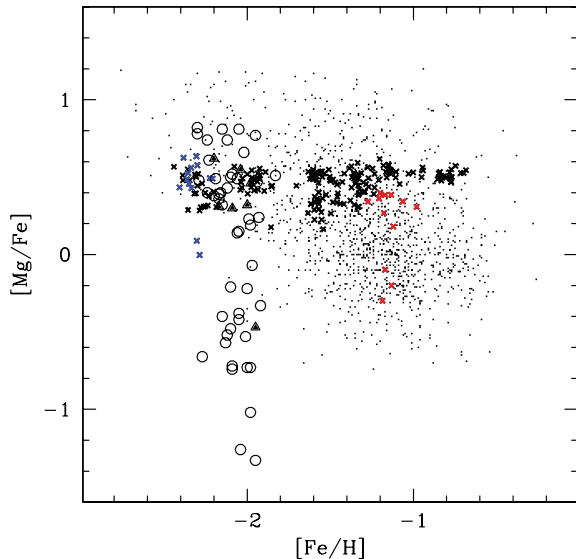
Figure 10. [Mg/Fe] versus [Fe/H] for (a) open circles: stars of NGC 2419 from this study, (b) triangles: stars of NGC 2419 from C11, (c) small dots: stars in the dwarf spheroidal satellites of the MW from Kirby et al. (2010), (d) × symbols: stars of various Galactic GCs from Carretta et al. (2009). Stars from NGC 7078 and NGC 2808 are plotted in blue and red, respectively, for reference, since they display the most Mg-deficient stars in the whole Carretta et al. (2009) sample.

(iii) an intrinsic dispersion of one (or more) of those elements that are electron donors. Hence, in deriving metallicities of individual stars from CaT lines, it seems advisable to countercheck also the abundance of Mg (which should be feasible to undertake in most cases, since the Mg I line at 8806.7 Å lies very close to the CaT), to validate the adopted calibration and avoid possible spurious effects as those described in Section 4.1.

8 SUMMARY

The main results derived from the analysis of 49 giant stars in NGC 2419 are summarized as follows.

(i) All the stars share the same iron content, with an average iron abundance of [Fe/H] = −2.09±0.02 dex (σ = 0.11 dex), where the observed dispersion is fully compatible with the uncertainties. Also, [Ca/Fe] and [Ti/Fe] turn out to be homogeneous.

(ii) NGC 2419 exhibits a large dispersion in the Mg abundance, reaching values of [Mg/Fe] ∼ −1 dex (unusual for GC stars). The large spread of Mg is likely the main origin of the observed dispersion of the CaT lines strength, previously interpreted as intrinsic dispersion in Ca or Fe. In fact, an Mg depletion leads to an increase of the equivalent widths of the CaT lines (at a constant Ca abundance). This effect is confirmed by the fact that the iron content inferred from the Ca triplet lines clearly anti-correlates with the Mg abundances. However, we bear in mind that the strength of the CaT lines suffers from the abundances of all the elements that are electron donors and the correct line profile for these lines should be derived by taking into account the global budget of the free electrons.

(iii) The [Mg/Fe] distribution is bimodal, with about 40 per cent of the stars having sub-solar [Mg/Fe] abundance ratio. This fraction is similar to that suggested by Di Criscienzo et al. (2011b) for the extreme population stars with initial helium abundance of $Y \simeq +0.4$, according to the horizontal branch morphology of the cluster.

(iv) A very large spread in the K content is detected among the stars of NGC 2419, spanning from solar values up to [K/Fe] ∼ 2 dex, with a bimodal distribution. A clearcut anti-correlation between [Mg/Fe] and [K/Fe] is observed, in agreement with the results already found by C11 for the star S1131 that shows an unusual depletion of Mg coupled with a strong enhancement of K.

Fig. 10 provides a direct illustration of the extremely unusual abundance pattern of NGC 2419. The spread in [Mg/Fe] is unrivalled both in GCs and in dwarf galaxies. A strong depletion of Mg is generally interpreted as due to a significant contribution of ejecta from SNIa to the gas from which Mg-poor stars are formed (see Tsujimoto & Bekki 2012, and references therein). Indeed, Fig. 10 shows that Mg depletion with increasing metallicity is a common feature in dwarf spheroidal (dSph) galaxies and that [Mg/Fe] < 0.0 stars are not rare in those systems. Lemasle et al. (2012) reports that the two most metal-rich stars in their sample of red giants in the Carina dSph have −0.6 < [Mg/Fe] < −1.0, not far from the most Mg-deficient stars in our NGC 2419 sample. However, the Mg depletion in dSph (as in any other galaxies studied until now) is always coupled with an increase of [Fe/H],[8] since the whole effect is due to SNIa enriching the interstellar medium with material that is Fe rich and poor in α elements, thus reducing the [Mg/Fe] ratio with respect to the pattern previously set up by SNII (see Tolstoy et al. 2009, for a recent review). This clearly does not occur in NGC 2419 where stars in the range −1.4 ≲ [Mg/Fe] ≲ +0.8 are indistinguishable in terms of [Fe/H].

This fundamental observational fact, coupled with the analogy of the bi-modalities in [Mg/Fe] and HB morphology recalled above, suggests as more likely the possibility that the observed pattern was produced by the same processes that cause the Na–O anti-correlations, and other signatures of the early chemical enrichment that are peculiar to GCs (Carretta et al. 2010a; Gratton et al. 2012). Further support to this hypothesis is provided by the fact that Mg-deficient stars lie systematically to the red of Mg-normal stars along the RGB, in the *V, U–V* CMD (Lardo et al., in preparation). In the framework of anti-correlations in GCs, Mg-deficient stars should correspond to Na-rich (and O-poor) stars and it is a generally observed characteristic of GCs to have Na-rich RGB stars that are redder than their Na-poor counterparts in CMDs that include the U band (see Lardo et al. 2011, for discussion and references). The colour difference is due to variations in the strength of CN and CH features at wavelengths lower than ∼4000 Å, that are driven by a variation of C and N abundance, that, in turn, are correlated with the abundance of other light elements tracing the self-enrichment process in GCs (like Na and O; Sbordone et al. 2011).

Even if the observed Mg spread can be attributed to this kind of processes, the reason for the extreme behaviour of this cluster, as well as the origin of the Mg–K anti-correlation, remains unclear. This latter feature, if confirmed, may shed new light into the whole process of GC formation, possibly providing a tool that may help to discriminate between competing models of self-enrichment (Decressin et al. 2007a,b; D'Ercole et al. 2008). An obvious singular characteristic of NGC 2419 is its distance from the centre of the Galaxy. Is it possible that a low degree of interaction with – for instance – the gas-rich disc of the MW has favoured the retention of enriched material in this cluster. Bellazzini et al. (2012) found some indirect evidence for the cluster having a significant larger

---

[8] As well as a star formation history lasting for a few Gyr (Tolstoy, Hill & Tosi 2009), clearly not observed in NGC 2419 (Di Criscienzo et al. 2011b; Bellazzini et al. 2012).

total mass in the past, as postulated by Di Criscienzo et al. (2011b) on a completely different basis: also a large total stellar mass may have played a role (but this is a general feature of models of GC formation accounting for the presence of multiple populations). In any case, this mysterious cluster does not cease to reveal new interesting features that makes it especially worthy of further study.

ACKNOWLEDGMENTS

REFERENCES

Alonso A., Arribas S., Martinez-Roger C., 1999, A&A, 140, 261
Andrievsky S. M., Spite M., Korotin S. A., Spite F., Bonifacio P., Cayrel R., Francois P., Hill V., 2010, A&A, 509, 88
Ashman K. M., Bird C. M., Zepf S. E., 1994, AJ, 108, 2348
Battaglia G., Irwin M., Tolstoy E., Hill V., Helmi A., Letarte B., Jablonka P., 2008, MNRAS, 383, 183
Baumgardt H., Kroupa P., Parmentier G., 2008, MNRAS, 384, 1231
Baumgardt H., Côté P., Hilker M., Rejkuba M., Mieske S., Djorgovski S. G., Stetson P., 2009, MNRAS, 396, 2051
Bellazzini M., 2007, A&A, 473, 171
Bellazzini M. et al., 2008, AJ, 136, 1147
Bellazzini M., Dalessandro E., Sollima A., Ibata R., 2012, MNRAS, 423, 844
Bessell M. S., 1979, PASP, 91, 589
Bragaglia A. et al., 2010, ApJ, 720, L41
Brodie J. P., Romanowski A. J., Strader J., Forbes D. A., 2011, AJ, 142, 199
Carlsson M., 1986, Uppsala Astronomical Observatory Reports 33
Carretta E., Bragaglia A., Gratton R., Lucatello S., 2009, A&A, 505, 139
Carretta E., Bragaglia A., Gratton R. G., Recio-Blanco A., Lucatello S., D'Orazi V., Cassisi S., 2010a, A&A, 516, 55
Carretta E., Bragaglia A., Gratton R., Lucatello S., Bellazzini M., D'Orazi V., 2010b, ApJ, 712, L21
Carretta E. et al., 2010c, A&A, 520, A95
Castelli F., Kurucz R. L., 2004, in Piskunov N., Weiss W. W., Gray D. F., eds, Proc. IAU Symp. Vol. 210, Modelling of Stellar Atmospheres. Astron. Soc. Pac., San Francisco, A20
Castelli F., 2005, Mem. Soc. Astron. Ital. Suppl., 8, 25
Cohen J. G., Kirby E. N., Simon J. D., Geha M., 2010, ApJ, 725, 288 (C10)
Cohen J. G., Huang W., Kirby E. N., 2011, ApJ, 740, 60 (C11)
Dalessandro E., Lanzoni B., Ferraro F. R., Vespe F., Bellazzini M., Rood R. T., 2008, ApJ, 681, 311
D'Antona F., Caloi V., Montalbán J., Ventura P., Gratton R., 2002, A&A, 395, 69
D'Antona F., Bellazzini M., Caloi V., Fusi Pecci F., Galleti S., Rodd R. T., 2005, ApJ, 631, 868

D'Ercole A., Vesperini E., D'Antona F., McMillan S. L., Recchi S., 2008, MNRAS, 391, 825
Decressin T., Meynet G., Charbonnel C., Prantzos N., Ekström S., 2007a, A&A, 464, 1029
Decressin T., Charbonnel C., Meynet G., 2007b, A&A, 475, 859
Di Criscienzo M. et al., 2011, AJ, 141, 81
Di Criscienzo M. et al., 2011, MNRAS, 414, 3381
Galleti S., Bellazzini M., Federici L., Buzzoni A., Fusi Pecci F., 2007, A&A, 471, 127
Gratton R., Carretta E., Bragaglia A., 2012, A&AR, 20, 50
Gray D. F., 1992, Cambridge Astrophys. Ser. Vol. 20, The Observation and Analysis of Stellar Spectra. Cambridge Univ. Press, Cambridge
Grevesse N., Sauval A. J., 1998, Space Sci. Rev., 85, 161
Gustafsson B., Edvarsson B., Eriksson K., Jorgensen U. G., Nordlund A., Plez B., 2008, A&A, 486, 951
Ibata R., Sollima A., Nipoti C., Bellazzini M., Chapman S. C., Dalessandro E., 2011a, ApJ, 738, 186 (I11a)
Ibata R., Sollima A., Nipoti C., Bellazzini M., Chapman S. C., Dalessandro E., 2011b, ApJ, 743, 43
Harris W. E., 1996, AJ, 112, 1487
Kirby E. N., Guhathakurta P., Bolte M., Sneden C., Geha M. C., 2009, ApJ, 705, 328
Kirby E. N. et al., 2010, ApJS, 191, 352
Lardo C., Bellazzini M., Pancino E., Carretta E., Bragaglia A., Dalessandro E., 2011, A&A, 525, A114
Laird J. B., Rupen M. P., Carney B. W., Latham D. W., 1988, AJ, 96, 1908
Lemasle B. et al., 2012, A&A, 538, A100
McCall M. L., 2004, AJ, 128, 2144
Mackey A. D., van den Bergh S., 2005, MNRAS, 360, 631
Martin N. F., Ibata R. A., Chapman S. C., Irwin M., Lewis G. F., 2007, MNRAS, 380, 281
Merle T., Thevenin F., Pichon B., Bigot L., 2011, MNRAS, 418, 863
Mucciarelli A., Origlia L., Ferraro F. R., Pancino E., 2009, ApJ, 695L, 134
Pietrinferni A., Cassisi S., Salaris M., Castelli F., 2004, ApJ, 612, 168
Piotto G. et al., 2007, ApJ, 661, L53
Pryor C., Meylan G., 1993, in Djorgovski S., Meylan G., eds, ASP Conf. Ser., 50, Structure and Dynamics of Globular Clusters. Astron. Soc. Pac., San Francisco, p. 357
Romano D., Karakas A. I., Tosi M., Matteucci F., 2010, A&A, 522, 32
Rutedge G. A., Hesser J. E., Stetson P. B., 1997, PASP, 109, 907
Sandquist E. L., Hess J. M., 2008, AJ, 136, 2259
Sbordone L., Bonifacio P., Castelli F., Kurucz R. L., 2004, Mem. Soc. Astron. Ital. Suppl., 5, 93
Sbordone L., 2005, Mem. Soc. Astron. Ital. Suppl., 8, 61
Sbordone L., Salaris M., Weiss A., Cassisi S., 2011, A&A, 534, A9
Shetrone M. D., Coté P., Sargent W. L. W., 2001, ApJ, 548, 592
Shetrone M. D., Siegel M. H., Cook D. O., Bosler T., 2009, AJ, 137, 62
Spite M., Spite F., Bonifacio P., Caffau E., Andrievsky S., Korotin S., Cayrel R., Francois P., 2011, SF2A-2011: Proc. Annual Meeting of the French Society of Astronomy and Astrophysics
Starkenburg E. et al., 2010, A&A, 513, 34
Stetson P. B., 2005, PASP, 117, 563
Takeda Y., Kaneko H., Matsumoto N., Oshino S., Ito H., Shibuya T., 2009, PASJ, 61, 563
Tolstoy E., Hill V., Tosi M., 2009, ARA&A, 47, 371
Tsujimoto T., Bekki K., 2012, ApJ, 751, L35
Walker M. G., Mateo M., Olszewski E. W., Bernstein R., Wang X., Woodroofe M., 2006, AJ, 131, 2114
Willman B., Strader J., 2012, AJ, 144, 76

This paper has been typeset from a TEX/LATEX file prepared by the author.